Structure and magnetic properties of Fe–Nb–B amorphous/nanocrystalline alloys produced by compaction of mechanically alloyed powders

J. J. Ipus, J. S. Blázquez, V. Franco, A. Conde, M. Krasnowski, T. Kulik, and S. Lozano-Pérez

Citation: Journal of Applied Physics **107**, 073901 (2010); doi: 10.1063/1.3319669
View online: http://dx.doi.org/10.1063/1.3319669
View Table of Contents: http://scitation.aip.org/content/aip/journal/jap/107/7?ver=pdfcov
Published by the AIP Publishing

Structure and magnetic properties of Fe–Nb–B amorphous/nanocrystalline alloys produced by compaction of mechanically alloyed powders

J. J. Ipus,[1] J. S. Blázquez,[1] V. Franco,[1] A. Conde,[1,a)] M. Krasnowski,[2] T. Kulik,[2] and S. Lozano-Pérez[3]
[1]*Departamento de Física de la Materia Condensada, ICMSE-CSIC, Universidad de Sevilla, P.O. Box 1065, 41080 Sevilla, Spain*
[2]*Faculty of Materials Science and Engineering, Warsaw University of Technology, ul. Wołoska 141, 02-507 Warsaw, Poland*
[3]*Department of Materials, University of Oxford, Parks Road, Oxford OX1 3PH, United Kingdom*

(Received 25 November 2009; accepted 19 January 2010; published online 2 April 2010)

Mechanical alloying of $Fe_{75}Nb_{10}B_{15}$ and $Fe_{85}Nb_5B_{10}$ systems has been performed from an initial mixture of elemental powders. A bcc supersaturated solid solution is developed during milling for both alloys. However, $Fe_{75}Nb_{10}B_{15}$ alloy also develops an amorphous phase, which amount increases with milling time. Milled powder samples were compacted at 7.7 GPa at different temperatures. Scanning electron microscopy images show that the presence of amorphous phase enhances the quality of compaction. Compaction at 823 K preserves both microstructure and magnetic properties of as-milled powders in both alloys. Compaction at 973 K affects mainly the crystalline fraction of the alloy with 10 at. % Nb. Compaction at 1273 K yields the formation of bcc Nb and fcc $Fe_{23}B_6$ phases, which magnetically harden the material. © *2010 American Institute of Physics*. [doi:10.1063/1.3319669]

I. INTRODUCTION

Nanocrystalline materials are extensively studied as advanced materials with improved physical properties. Among them, the Nanoperm-type alloys have received much attention because these materials show excellent soft magnetic properties and can be used extensively in commercial applications.[1,2] These good soft magnetic properties depend on the microstructure of material,[3–5] so the structural characterization is very important in order to understand the physical behavior of the system.

Mechanical alloying has become a very versatile technique to directly produce metastable microstructures (amorphous, nanocrystalline, supersaturated solid solutions, etc.)[6] from elemental powders or alloys. This technique allows us to obtain easily (and economically) a large amount of processed material. However, it is necessary to compact this nanocrystalline powders to form bulk samples to cover practical requirements, being an important task to preserve the nanocrystalline microstructure and the magnetic properties of powder samples.

In this work, mechanical alloying of $Fe_{75}Nb_{10}B_{15}$ and $Fe_{85}Nb_5B_{10}$ powders have been performed, and their morphology, composition, microstructure, and magnetic properties studied as a function of milling time. At the end of the studied milling time, partially amorphous and nanocrystalline powders were compacted at different temperatures. Changes in microstructure, thermal stability, and magnetic properties were studied as a function of these compaction temperatures, in order to establish a limit to preserve the powder microstructure after consolidation for these alloys.

a)Author to whom correspondence should be addressed.: Tel.: (34) 95 455 28 85. FAX: (34) 95 461 20 97. Electronic mail: conde@us.es.

II. EXPERIMENTAL

$Fe_{75}Nb_{10}B_{15}$ and $Fe_{85}Nb_5B_{10}$ compositions were prepared by ball milling in a shaker mill (Spex 8000D) from pure crystalline powders of Fe, Nb, and B (>99% purity). For simplicity, the studied alloys will be named in the following by their Nb content: Nb10 for $Fe_{75}Nb_{10}B_{15}$ and Nb5 for $Fe_{85}Nb_5B_{10}$. The initial powder mass was 10 g and the ball to powder ratio was 12:1. After selected times some amount of powder was taken out from the vials to characterize the morphology, composition, microstructure, thermal stability, and magnetic properties evolution. Powder handling and milling was carried out under argon atmosphere.

Particle size distribution and morphology was studied by scanning electron microscopy (SEM) in a Jeol JSM-6460 LV operated at 30 kV. Compositional evolution was studied by energy dispersive x-ray (EDX) analysis using an Oxford instruments Incax-sight detector using stationary spots at the center of each probed particle. Identification of present phases and microstructure characterization were studied by x-ray diffraction (XRD), using Cu $K\alpha$ radiation, and by Mössbauer spectrometry. Crystal size and microstrain were obtained from a single peak fitting. Assuming that the full breadth of the (110) maximum of bcc Fe is only due to grain size, a minimum grain size is obtained and if this full breadth is only ascribed to microstrains, a maximum value of this parameter is obtained. Mössbauer spectra were recorded at room temperature in a transmission geometry using a $^{57}Co(Rh)$ source. Values of hyperfine parameters were obtained by fitting with NORMOS program[7] and the isomer shift was quoted relative to that of α-Fe at room temperature. Local microstructure was studied by transmission electron microscopy (TEM) in a Jeol JEM3000F operated at 297 kV and equipped with an electron energy loss spectrometer

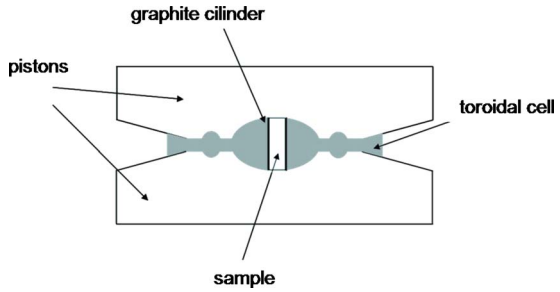

FIG. 1. (Color online) Schematic view of the high pressure cell of UNIPRESS.

(EELS) which enables the detection of B. TEM samples were prepared following the lift out procedure[8] using a focus ion beam (FIB) FEI 200 to extract, from a powder particle, a slice of area $\sim 10 \times 6$ μm^2 and thin enough to be electron transparent. TEM studies on compacted bulk samples were performed in a Philips CM200 operated at 200 kV. TEM samples were thinned using a Gatan Duo Ion mill.

Thermal characterization of the samples was studied by differential scanning calorimetry (DSC) using a Perkin–Elmer DSC7 in Ar atmosphere. Magnetic properties were studied in a Lakeshore 7407 vibrating sample magnetometer with maximum applied field of 15 kOe. Hysteresis loops were obtained at room temperature and magnetization curves in a temperature range from 77–420 K. Powder samples were consolidated in form of cylinders of ~ 5 mm diameter and ~ 3 mm high using a press equipped with a toroid-type high pressure cell. The shape of the cell and the material of the gasket ensured that the compacting conditions were close to isostatic ones (see Fig. 1 and Ref. 9). The compaction process was performed at 7.7 GPa and different temperatures (823, 973, and 1273 K). The loading, at a rate of 0.5 GPa/min, was done prior to the heating. The heating and cooling rate was 1000 K/min.

III. RESULTS AND DISCUSSION

After 40 h milling, an average particle size of ~ 180 and ~ 70 μm for Nb10 and Nb5, respectively, was measured from SEM images. The compositional evolution was followed from EDX, finding that, after 40 h milling, the majority of the particles has a composition close to the nominal one but a dispersion of ~ 10 at. % Fe still remains.

In Fig. 2, XRD patterns of samples after several milling times are shown for both alloys. The formation of a supersaturated bcc Fe(Nb,B) solid solution at intermediate times can be detected for both alloys. In the case of Nb5 alloy, this microstructure is preserved up to the end of the explored range. However, in the case of Nb10 alloy, besides the supersaturated solid solution, the formation of an amorphous phase is indicated by the presence of a characteristic amorphous halo in the patterns. The evolution of lattice parameter, minimum crystal size, maximum microstrain, and crystalline fraction of bcc Fe(Nb,B) solid solution can be studied, as is depicted in Fig. 3. An important increase in lattice parameter can be observed [Fig. 3(a))] when the supersaturated solid solution is formed for both alloys, ~ 10 h milling, as well as a significant refinement in the minimum crystal size [Fig. 3(b)] and an increase in the maximum microstrains [Fig. 3(c)]. For longer times, the lattice parameter increases again, being higher for Nb10 alloy. The minimum crystal size and maximum microstrains are almost the same, $D_{min} \sim 5$ nm and $\varepsilon_{max} < 2\%$, respectively, for both alloys.

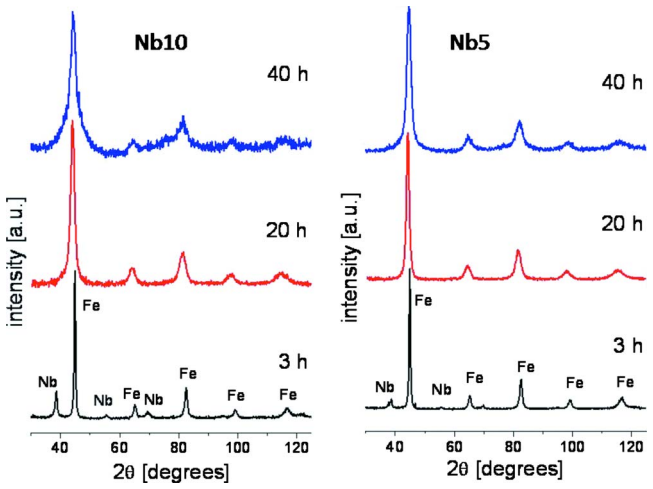

FIG. 2. (Color online) XRD patterns of as-milled samples as a function of milling time for both alloys, (left) Nb10 and (right) Nb5.

Figure 3(d) shows the evolution of crystalline fraction, X_C (obtained from a deconvolution of the (110) diffraction maximum of the bcc phase and the amorphous halo), as a function of milling time for Nb10 alloy. After the formation of solid solution, the crystalline fraction of bcc Fe(Nb,B) decreases continuously down to $X_C \sim 40\%$ at the end of the studied range, ascribed to the formation of amorphous phase. With the appearance of amorphous phase, an increase in the fraction of Fe environments with low field contributions is observed in Mössbauer spectra of Nb10 alloy (Fig. 4), sug-

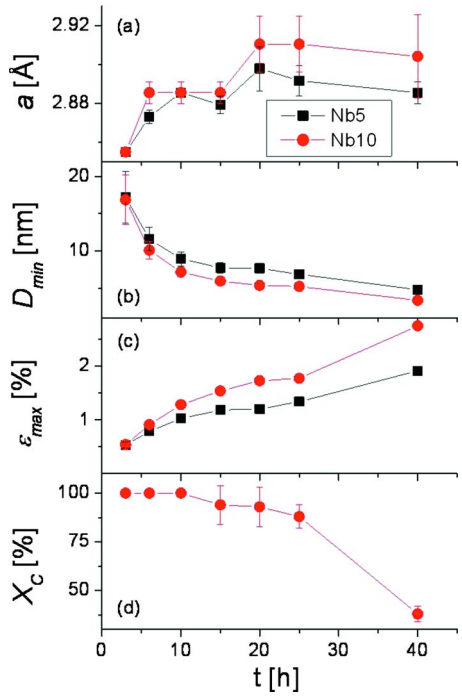

FIG. 3. (Color online) (a) Lattice parameter, (b) minimum crystal size, (c) maximum microstrain, and (d) crystalline fraction of bcc Fe(Nb,B) type phase as a function of milling time.

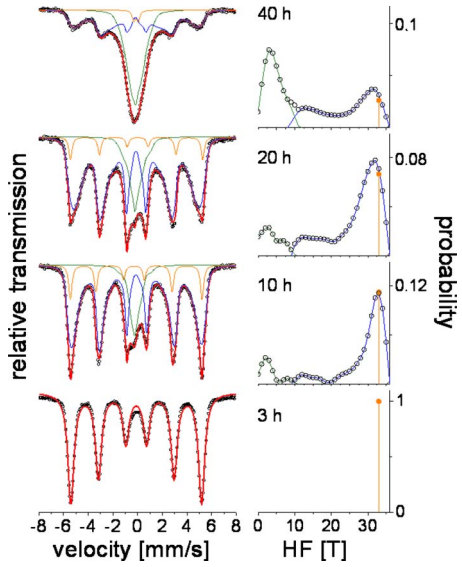

FIG. 4. (Color online) Mössbauer spectra and hyperfine field distributions as a function of milling time for Nb10 alloy.

gesting that this amorphous phase is paramagnetic at room temperature as the fitting procedure cannot distinguish the very low field contribution (<5 T) from paramagnetic contributions in such complex system as the one studied here. Superparamagnetic behavior of the nanocrystals contributing to the Mössbauer spectra could be discarded, as the characteristic measuring time for this technique is very short $\sim 10^{-8}$ s.[10]

Figure 5(a) shows a secondary electron FIB image of the TEM sample prepared by the lift out procedure. Prior to the Ga^+ milling, and in order to avoid damage of the sample, a protective Pt layer was deposited on top of the particle. Finally, once the sample is cut and with the help of a micromanipulator, the sample is welded to a Cu grid using Pt. Figure 5(c) shows bright field images of Nb10 alloy after 40 h milling, where a uniform nanocrystalline matrix, identified

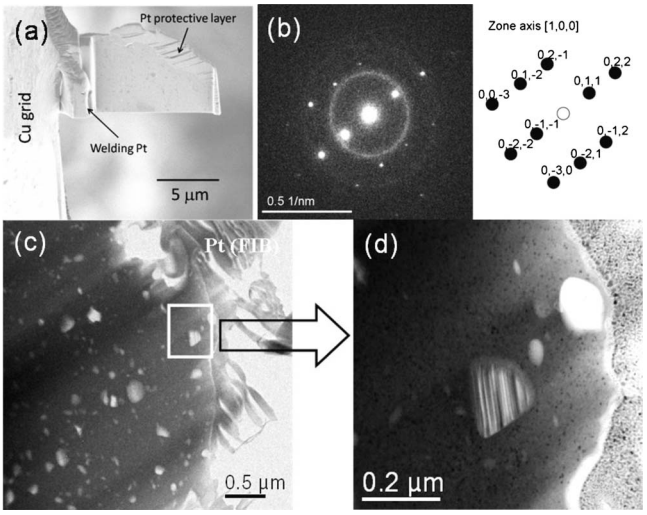

FIG. 5. (a) Secondary electron FIB image of the TEM sample prepared by lift out procedure; (b) SAD pattern of a boron inclusion along with a possible indexation using a tetragonal structure; (c) bright field TEM images of the Nb10 alloy after 40 h milling; and (d) magnified view of the rectangle in the left image (c).

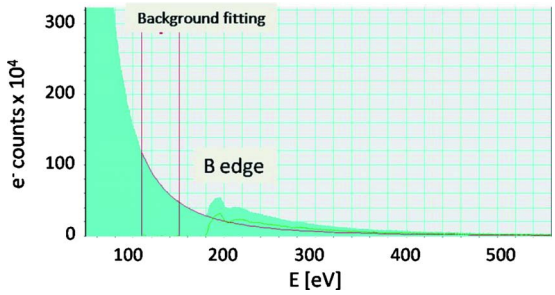

FIG. 6. (Color online) EELS spectrum of a boron inclusion.

as bcc Fe(Nb,B) by using selected area diffraction (SAD) patterns [Fig. 5(b)], was observed together with larger bright inclusions randomly dispersed throughout the sample. The almost pure B composition of these inclusions was confirmed by EELS, as shown in Fig. 6. The crystalline nature of these B inclusions was confirmed by SAD, as shown in Fig. 5(b), finding that their microstructure (interplanar distances are $d_1=5.6$ and $d_2=3.9$ Å with an angle of 75.5°) is coherent with that detected previously in powder of the same composition obtained in a planetary mill.[11]

Magnetization measurements confirm the biphasic character of Nb10 alloy observed by XRD and Mössbauer. Figure 7 shows the temperature dependence of saturation magnetization for samples of Nb10 alloy after two milling times. At low temperatures, it can be observed that saturation magnetization of the sample decreases as milling time increases due to the higher value of magnetization of crystalline phase with respect to amorphous phase. Moreover, the Curie temperature of this amorphous phase (calculated from the inflexion point of magnetization curves) is close to room temperature, $T_C \sim 270$ K. This Curie temperature is slightly higher than that measured for samples with similar composition but milled under different conditions,[12] which could be mainly explained by the absence of Cr as contamination during this milling and the presence of tiny amounts of Ni.

The powder samples for both alloys after 40 h milling (as-milled samples) were compacted under isostatic conditions at 7.7 GPa and different temperatures (823, 973, and 1273 K), leading to bulk samples with a density of ~ 7.5 g/cm^3. Figure 8 shows SEM images of the surface of bulk samples, where it can be seen that Nb5 samples present

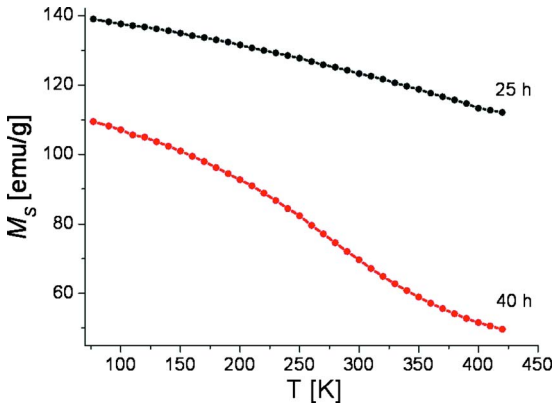

FIG. 7. (Color online) Temperature dependence of saturation magnetization of Nb10 alloy after two selected milling times.

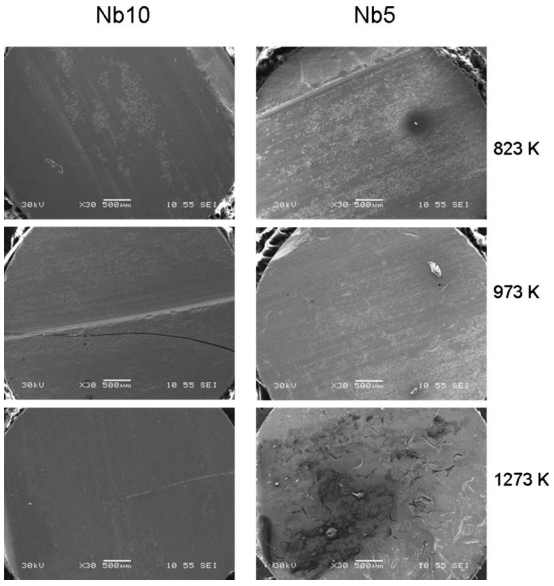

FIG. 8. SEM images of the compacted samples for the different compaction temperatures studied.

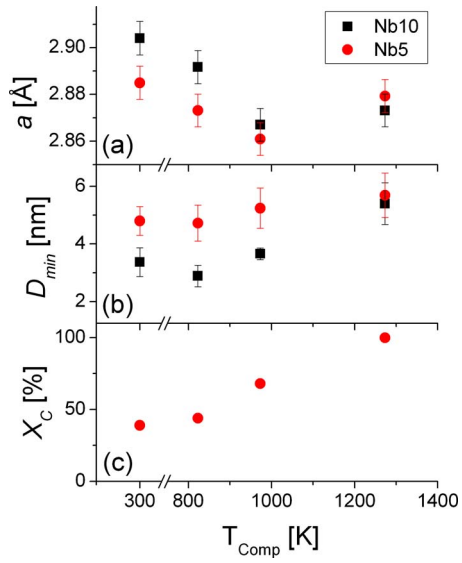

FIG. 10. (Color online) (a) Lattice parameter, (b) minimum crystal size of bcc Fe(Nb,B) type phase, and (c) crystalline fraction as a function of compaction temperature. The as-milled samples (300 K) are presented for comparison.

a huge amount of cracks and pores on its surface unlike Nb10 samples, which suggests that the presence of amorphous phase in the powder microstructure favors its compaction quality, even not being fully amorphous.

XRD patterns were collected on samples of both alloys after each compaction temperature as shown in Fig. 9. They show a similar lattice parameter of bcc Fe(Nb,B) phase after compaction at 823 K to that of as-milled sample for both alloys [Fig. 10(a)]. Moreover, a slight reduction is observed after compaction at 973 K due to purification of bcc Fe phase. For samples compacted at 1273 K, new diffraction maxima are detected for both alloys, which correspond to bcc Nb and fcc $Fe_{23}B_6$ (Ref. 13) phases, although, the presence of bcc Nb is more clear for Nb10 alloy. The last patterns were fitted using the Pawley method.[14]

The compaction temperature does not show any important effect on the minimum crystal size for both alloys with respect to values of as-milled powder [Fig. 10(b)], showing a slight increase with the temperature but remaining in the nanocrystalline scale. Moreover, the crystalline fraction for Nb10 alloy after compaction at 823 K, $X_C=41\pm2\%$, is similar to the value observed for as-milled sample. For higher compaction temperatures, an important evolution is observed in crystalline fraction, $X_C=68\pm4\%$ and 100% for 973 and 1273 K, respectively, as shown in Fig. 10(c).

TEM results confirm the results derived from XRD on compacted samples. Figure 11(a) shows a bright field image, where amorphous, nanocrystals, and boron inclusions can be observed. Since this bright field image contained lattice contrast, a Fourier transform of a square region on the boron inclusion is shown in Fig. 11(c). This Fourier transform confirms the crystalline character of the boron inclusions. At Fig. 11(b) a SAD pattern showing the bcc Fe(Nb) diffraction rings is shown.

From DSC scans, a crystallization temperature of ~850 K was measured for the amorphous phase developed during milling of Nb10 composition in a planetary mill,[15] which could explain the weak evolution of X_C after compaction at 823 K (below crystallization temperature). Moreover, both onset temperatures and activation energies of crystalli-

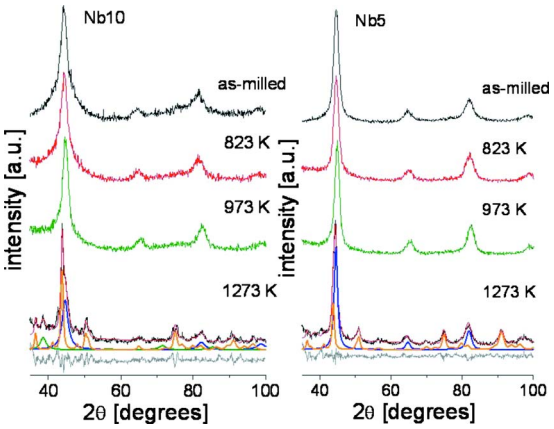

FIG. 9. (Color online) XRD patterns as a function of compacted temperature for both alloys. For alloys compacted at 1273 K, the Pawley fit is shown.

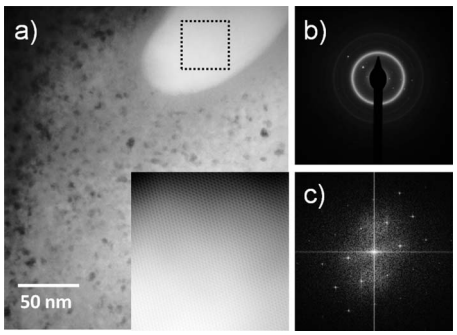

FIG. 11. (a) Bright field image of Nb10 alloy compacted at 823 K. The inset is an enlarged image of the square region; (b) SAD pattern of the same sample. Rings corresponds to bcc Fe(Nb) phase, spots might correspond to B inclusions; and (c) Fourier transform of boron inclusion (square region in BF image).

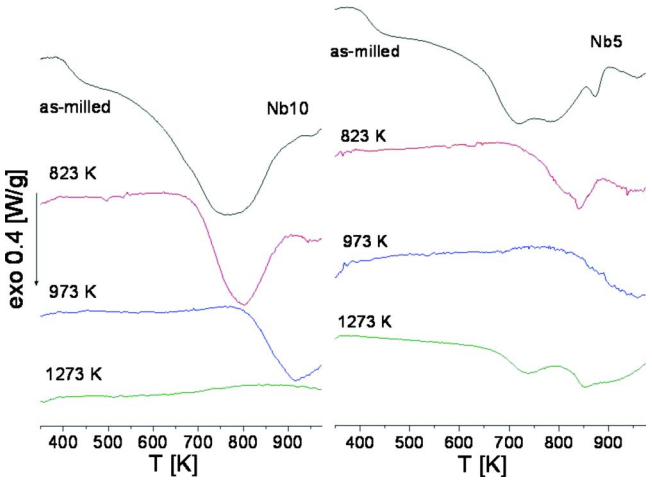

FIG. 12. (Color online) DSC scans of compacted samples and as-milled ones at 40 K/min for both alloys. Subtraction of baseline was performed using a second run.

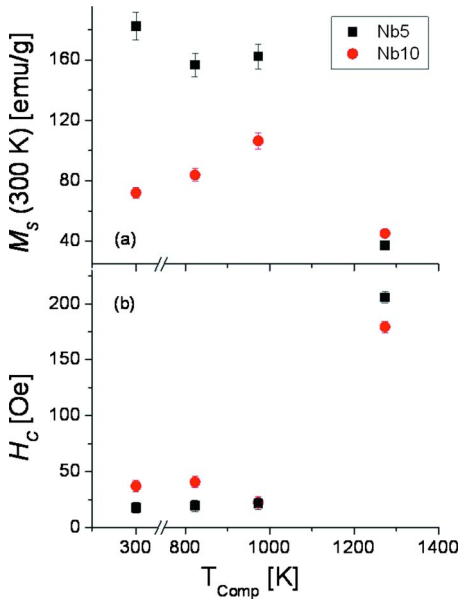

FIG. 13. (Color online) Magnetic properties, (a) saturation magnetization and (b) coercive field as a function of compaction temperature. The as-milled samples are presented for comparison.

zation processes increase as the pressure increases in some nanocrystalline systems compacted in similar conditions,[16] which could explain that, even after compaction at 973 K (above the crystallization temperature at room pressure), the bulk sample still presents amorphous phase.

Figure 12 shows DSC scans of samples at different compaction temperatures as well as that of as-milled powders for both alloys. It can be observed that the broad exothermic peak, typical of powder samples,[15] reduces its enthalpy from 320 ± 5 to 130 ± 5 J/g and from 230 ± 5 to 64 ± 5 J/g, for Nb10 and Nb5, respectively, after compaction at 823 K with respect to as-milled samples. As this temperature does not produce microstructural changes, this enthalpy change should be ascribed to relaxation processes of the powder samples during hot compaction. Finally, DSC scans of bulk samples compacted at 1273 K show a more stable microstructure for Nb10 alloy than for Nb5 alloy, which DSC scan exhibits two exothermic events at ~750 and ~850 K. These processes could be ascribed to a less thermal stability of the fcc $(FeNb)_{23}B_6$ type phase detected for this alloy due to the introduction of Nb atoms into boride phase, although when this phase appears after crystallization of amorphous ribbons it is stable up to higher temperatures[17,18] and the Nb content in the fcc boride phase developed in Nb10 alloy is expected to be enriched in Nb with respect to Nb5. These exothermic peaks could be some residual of the energy stored in the powder particles (the temperature range is similar to that found in as-milled samples), which due to the low quality of compaction of the Nb5 sample at 1273 K was not completely released as occurred in Nb10 alloy.

The magnetic properties at room temperature as a function of compaction temperature are shown in Fig. 13. It can be observed a reduction of ~15% in saturation magnetization for bulk samples of Nb5 alloy compacted at 973 K with respect to the as-milled one. However, in the case of Nb10 alloy, an increase in saturation magnetization is observed for these temperatures due to the increase in crystalline fraction and the purification of bcc Fe phase observed at this temperature range. After compaction at 1273 K, a decrease in saturation magnetization is observed for both alloys, which could be ascribed to the formation of $(FeNb)_{23}B_6$ phase.

The coercive field has not changed significantly in bulk samples compacted at temperatures lower than 1273 K with respect to as-milled samples for both alloys. However, samples compacted at 1273 K shows an increase in coercive field due to the formation of $(FeNb)_{23}B_6$ phase. In fact, it has been shown that the precipitation of boride-type phases can pin the wall domains leading to a strong increase in coercive field.[19,20]

IV. CONCLUSIONS

Mechanical alloying of $Fe_{75}Nb_{10}B_{15}$ and $Fe_{85}Nb_5B_{10}$ powders followed by compaction as well as characterization of microstructure and magnetic properties of bulk samples were studied. Morphology, composition, microstructure, and magnetic properties evolution as a function of milling time were followed. Compacted samples were obtained from milled powders under 7.7 GPa isostatic pressure and at different temperatures. Changes in microstructure, thermal stability, and magnetic properties of these samples with respect to as-milled ones have been studied as a function of compaction temperature.

The average powder particle size at the end of milling time studied is smaller for the alloy with the lowest Nb content. At long milling times, the composition of powder particles is close to the nominal one but a dispersion of ~10% in the Fe content was found.

Combining of XRD, Mössbauer and TEM results shows that the alloy with the lowest Nb content only develops a bcc Fe(Nb,B) supersaturated solid solution and almost pure B inclusions, whereas the alloy with highest Nb content also develops an amorphous phase.

Saturation magnetization measurements reveal that the

magnetization of amorphous phase is lower than that of crystalline phase. Moreover, the Curie temperature of the amorphous phase is close to room temperature.

The presence of amorphous phase enhances the quality of compaction. After compaction at 823 K, bulk samples preserve the microstructure and magnetic properties of as-milled powders for both alloys. Compaction at 973 K, mainly affects the amount of amorphous phase developed in the powder sample of the alloy with 10 at. % Nb but no new phases are formed. After compaction at 1273 K, the formation of bcc Nb and fcc $Fe_{23}B_6$ phases are detected leading to deterioration of soft magnetic properties of bulk samples.

Although bulk samples were successfully obtained from compaction of milled powders in both alloys, the presence of amorphous phase leads to a better quality of compaction even at high temperature, when the amorphous phase crystallizes and is no longer detected in the final product.

From the functional point of view, compacting the samples which have amorphous phase leads to qualities of compaction as good as that of samples compacted at higher temperatures, whereas the microstructure and good soft magnetic properties are preserved.

ACKNOWLEDGMENTS

This work was supported by the Spanish Ministry of Science and Innovation (MICINN) and EU FEDER (Project No. MAT2007-65227) and the PAI of the Regional Government of Andalucía (Project No. P06-FQM-01823). J.J.I. acknowledges a fellowship from MICINN. J.S.B. acknowledges a research contract from Junta de Andalucía. The TEM investigations were partially supported by the IP3 project of the 6th Framework Programme of the European Commission: ESTEEM Contract No. 026019.

The authors would like to thank to Dr. S. Gierlotka (Institute of High Pressure Physics of the Polish Academy of Sciences, Warsaw, Poland) for assistance in performing the hot-pressing consolidation.

[1] A. Makino, T. Hatanai, A. Inoue, and T. Matsumoto, Mater. Sci. Eng., A **226–228**, 594 (1997).
[2] M. E. McHenry, M. A. Willard, and D. E. Laughlin, Prog. Mater. Sci. **44**, 291 (1999).
[3] A. Hernando, M. Vázquez, T. Kulik, and C. Prados, Phys. Rev. B **51**, 3581 (1995).
[4] I. Chicinas, N. Jumate, and G. Matei, J. Magn. Magn. Mater. **140–144**, 1875 (1995).
[5] S. Szabó, D. L. Beke, L. Harasztosi, L. Daróczi, G. Posgay, and M. Kis-Varga, Nanostruct. Mater. **9**, 527 (1997).
[6] C. Suryanarayana, Prog. Mater. Sci. **46**, 1 (2001).
[7] R. A. Brand, J. Lauer, and D. M. Herlach, J. Phys F: Met., Phys. **13**, 675 (1983).
[8] B. I. Prenitzer, L. A. Giannuzzi, K. Newman, S. R. Brown, R. B. Irwin, T. L. Shofner, and F. A. Stevie, Metall. Mater. Trans. A **29**, 2399 (1998).
[9] http://www.unipress.waw.pl/nano/index.php?option=com_content&task=view&id=23&Itemid=22
[10] G. C. Papaefthymiou, Nanotoday **4**, 438 (2009).
[11] J. J. Ipus, J. S. Blázquez, S. Lozano-Pérez, and A. Conde, Philos. Mag. **89**, 1415 (2009).
[12] J. J. Ipus, J. S. Blázquez, V. Franco, A. Conde, and L. F. Kiss, J. Appl. Phys. **105**, 123922 (2009).
[13] J. S. Blázquez, S. Lozano-Pérez, and A. Conde, Philos. Mag. **82**, 409 (2002).
[14] G. S. Pawley, J. Appl. Crystallogr. **14**, 357 (1981).
[15] J. J. Ipus, J. S. Blázquez, V. Franco, and A. Conde, Intermetallics **16**, 1073 (2008).
[16] H. Dimitrov, J. S. Blázquez, J. Latuch, and T. Kulik, Intermetallics **15**, 891 (2007).
[17] J. S. Blázquez, C. F. Conde, and A. Conde, J. Non-Cryst. Solids **287**, 187 (2001).
[18] J. S. Blázquez, C. F. Conde, and A. Conde, Appl. Phys. Lett. **79**, 2898 (2001).
[19] T. Reininger, B. Hofmann, and H. Kronmuller, J. Magn. Magn. Mater. **111**, L220 (1992).
[20] V. Franco, C. F. Conde, and A. Conde, J. Magn. Magn. Mater. **185**, 353 (1998).